Dalton Transactions

PAPER

View Article Online
View Journal | View Issue

Cite this: *Dalton Trans.*, 2018, **47**, 429

Experimental and theoretical studies on the NLO properties of two quaternary non-centrosymmetric chalcogenides: $BaAg_2GeS_4$ and $BaAg_2SnS_4$†

Hong Chen,[a] Pei-Fei Liu,[b,c] Bing-Xuan Li,[d] Hua Lin,*[a] Li-Ming Wu*[a,e] and Xin-Tao Wu[a]

New middle and far-infrared (MFIR) nonlinear optical (NLO) chalcogenides have been receiving increasing attention for their great importance in military and civil fields. In addition, the current challenge in the efforts for identifying a promising MFIR NLO material lies in achieving simultaneously large second-harmonic generation (SHG) intensity and high laser-induced damage threshold (LIDT) in the same material. In this study, two quaternary non-centrosymmetric (NCS) sulfides, $BaAg_2GeS_4$ (**1**) and $BaAg_2SnS_4$ (**2**), were synthesized from a high-temperature solid-state reaction using $BaCl_2$ flux in evacuated closed silica tubes. Although **1** and **2** show identical stoichiometry, they crystallize in different NCS space groups, tetragonal $I\bar{4}2m$ (no. 121) and orthorhombic $I222$ (no. 23), respectively, based on the results of crystal structure solution. In their structures, highly distorted AgS_4 tetrahedra interconnect together *via* corner-sharing to form two-dimensional (2D) layers, which are further bridged with isolated GeS_4 or SnS_4 units to produce a three-dimensional (3D) framework structure with Ba cations lying in the tunnels. Remarkably, they not only possess phase-matchable (PM) abilities but also exhibit a good balance between strong SHG responses (1.7× and 0.4× $AgGaS_2$) and high LIDTs (3.2× and 1.5× $AgGaS_2$). Moreover, theoretical calculations based on density functional theory (DFT) methods have aided the understanding of energy bands, electronic structures, and linear and NLO properties.

Received 6th November 2017,
Accepted 25th November 2017

DOI: 10.1039/c7dt04178k

rsc.li/dalton

Introduction

As crucial frequency-conversion components in solid-state lasers, second-order nonlinear optical (NLO) crystals have attracted increasing attention in the fields of civilian and military applications.[1] Until recently, there have been already numerous commercial second-order NLO materials that satisfied the practical application requirements in the ultraviolet–visible (UV–Vis) and near-infrared (NIR) regions, such as KH_2PO_4 (KDP),[2] β-BaB_2O_4 (BBO),[3] LiB_3O_5 (LBO)[4] and $LiNbO_3$ (LNO).[5] In contrast, only a few commercially available second-order NLO crystals [*e.g.*, chalcopyrite-like semiconductors $ZnGeP_2$,[6] $AgGaSe_2$ [7] and $AgGaS_2$ (AGS)[8]] are available in the middle and far-infrared (MFIR) region. Unfortunately, these crystals still possess a series of inherent performance defects, including harmful two-photon absorption (TPA), non-phase-matching (NPM) behaviour (small birefringence Δn) or low laser-induced damage threshold (LIDT), which seriously hinder their widespread applications.[9] Therefore, the development and exploration of new high-performance MFIR NLO materials is of great significance and challenging in the field of science and technology.

The prerequisite of a NLO material is that it should possess crystallographically non-centrosymmetric (NCS) structure. In the past decades, NCS metal-chalcogenides with two or more types of asymmetric building units have been receiving unprecedented attention not only for their fascinating structural features but also for their excellent NLO properties (*e.g.*, strong second harmonic generation (SHG) response, high LIDT, suit-

[a]*State Key Laboratory of Structural Chemistry, Fujian Institute of Research on the Structure of Matter, Chinese Academy of Sciences, Fuzhou, Fujian 350002, People's Republic of China. E-mail: linhua@fjirsm.ac.cn, liming_wu@fjirsm.ac.cn*
[b]*Institute of High Energy Physics, Chinese Academy of Sciences (CAS), Beijing 100049, China*
[c]*Dongguan Neutron Science Center, Dongguan 523803, China*
[d]*Key Laboratory of Optoelectronic Materials Chemistry and Physics, Fujian Institute of Research on the Structure of Matter, Chinese Academy of Sciences, Fuzhou, Fujian 350002, People's Republic of China*
[e]*Key Laboratory of Theoretical and Computational Photochemistry, Ministry of Education, College of Chemistry, Beijing Normal University, Beijing 100875, People's Republic of China*

†Electronic supplementary information (ESI) available: Additional EDX, PXRD, calculation results, together with additional figures. See DOI: 10.1039/C7DT04178K

able Δn, and wide MFIR transparency range).[10–43] The well-known examples include $Li_2Ga_2GeS_6$,[10] Li_2CdGeS_4,[11] $Li_4HgGe_2S_7$,[12] $Na_2ZnGe_2S_6$,[13] $NaGaIn_2Se_5$,[14] $Cs_5BiP_4Se_{12}$,[15] $CsM^{III}Sn_2Se_6$ (M^{III} = Ga, In),[16] $AZrPQ_6$ (A = K–Cs; Q = S, Se),[17] $A_3Ta_2AsS_{11}$ (A = K, Rb),[18] $A_4GeP_4Q_{12}$ (A = K–Cs; Q = S, Se),[19] $A_2Hg_3M^{IV}_2S_8$ (A = Na, K, Rb; M^{IV} = Si, Ge and Sn),[20] $[AX_3][Ga_3PS_8]$ (A = K, Rb; X = Cl, Br),[21] $AM^{II}_4M^{III}_5Q_{12}$ (A = K–Cs; M^{II} = Mn, Zn, Cd, Hg; M^{III} = Ga, In; Q = S, Se),[22] $PbGa_2M^{IV}Se_6$ (M^{IV} = Si, Ge),[23] $Ba_6Li_2CdSn_4S_{16}$,[24] $Ba_{23}Sb_2Ga_8S_{38}$,[25] $Ba_4CuGa_5Q_{12}$ (Q = S, Se),[26] $Ba_6Ag_{2.67+4y}Sn_{4.33-y}S_{16-x}Se_x$,[27] $BaGa_2SnSe_6$,[28] $Ba_5CdGa_6Se_{15}$,[29] $Ba_6Zn_7Ga_2S_{16}$,[30] Sm_4GaSbS_9,[31] La_4InSbS_9,[32] $La_3GaGe_{0.5}S_7$,[33] and $AgGa_2PS_6$.[34] In the recent studies, Pan *et al.* carried out detailed exploratory synthesis on the quaternary Ba–M^I_2–M^{IV}–Q_4 system (M^I = Li, Na, Cu; M^{IV} = Si, Ge, Sn; Q = S, Se) and discovered a series of novel MFIR NLO candidates.[44] Interestingly, these studies indicated that the slight change in cation size (M^I or M^{IV} atoms) would result in different structural features, further affecting their NLO performances. For instance, $BaLi_2M^{IV}Q_4$ compounds show large SHG efficiencies with compressed chalcopyrite-like (CCL) structures and all of them exhibit the PM abilities,[44c] while $BaCu_2M^{IV}Q_4$ crystallizes in three different space groups and they exhibit the NPM behavior.[44b]

With the above considerations in mind, we focused our investigations on the quaternary Ba/M^I/M^{IV}/S system and successfully obtained two Ag-containing compounds, $BaAg_2GeS_4$ and $BaAg_2SnS_4$. Crystal structures of these two compounds were first characterized by Teske *et al.* in 1976 [45] and 1979,[46] respectively, but their critical NLO properties (*e.g.*, SHG, LIDT or Δn) have not been reported. In this paper, the synthesis, structural comparison and thermal stability are systemically presented. Moreover, the SHG responses, LIDTs as well as theoretical NLO properties are presented for the first time.

Experimental section

Materials and methods

All of the chemicals were obtained from commercial sources and used without further purification. Ba rod (2 N), Ag powder (3 N), Ge shot (5 N), Sn shot (5 N) and S powder (5 N) were purchased from Alfa-Aesar. It should be noted that the external oxide layer on the surface of Ba rod, which is used as a reagent, needs to be thoroughly scraped before use. Powder X-ray diffraction (PXRD) patterns were measured on the Rigaku Mini-Flex II powder diffractometer using Cu-K_α radiation (λ = 1.5416 Å) at room temperature, and the 2-theta range was from 10 to 70° with a step size of 0.02°. The semi-quantitative energy-dispersive X-ray (EDX, Oxford INCA) spectra were recorded on a field emission scanning electron microscope (FESEM, JSM6700F). The UV–Vis–NIR diffuse reflectance spectra were performed at room temperature using a PerkinElmer Lambda 950 UV–Vis spectrophotometer in the wavelength range of 190–2500 nm and $BaSO_4$ was used as a standard. The absorption spectra were calculated from the reflection spectra according to the Kubelka–Munk function: $\alpha/S = (1-R)^2/2R$, where α is the absorption coefficient, S is the scattering coefficient and R is the reflectance.[47] The thermal stability analyses were carried out with a NETZSCH STA 449C simultaneous analyser and heated from 300 to 1273 K at a rate of 10 K min^{-1} under a constant flow of nitrogen atmosphere.

Syntheses

After a series of explorations on the experimental conditions, including annealing temperature, starting reactant and loading ratio, the optimal synthesis route is as follows. The chemicals were loaded in fused silica tubes and sealed under vacuum (<10^{-3} Pa). The tubes were heated at 573 K for 20 h, raised to 1173 K and maintained for 100 h; then they were cooled to 473 K at 3 K h^{-1} before turning off the furnace. For compound **1**, dark-red irregular bulk crystals were obtained by reacting 1.0 mmol Ba, 2.0 mmol Ag, 1.0 mmol Ge, 4.0 mmol S, and 2.7 mmol $BaCl_2$. For compound **2**, black irregular bulk crystals were obtained by reacting 1.0 mmol Ba, 2.0 mmol Ag, 1.0 mmol Sn, 4.0 mmol S and 3.1 mmol $BaCl_2$. The results of EDX analyses on several single crystals gave average molar ratios of Ba/Ag/M/S of 1/2.1(3)/1.0(1)/4.1(2) for compound **1** and 1/2.1(2)/1.1(3)/4.0(1) for compound **2** (ESI, Fig. S1†), respectively, which are in good agreement with those determined from single-crystal XRD data. The products with a yield of about 95% for compound **1** and 90% for compound **2** were obtained after washing with deionized water to remove the $BaCl_2$ flux and soluble by-products, and dried with ethanol in air. The homogeneous target products were obtained as indicated by the PXRD patterns shown in Fig. 1 and no impure

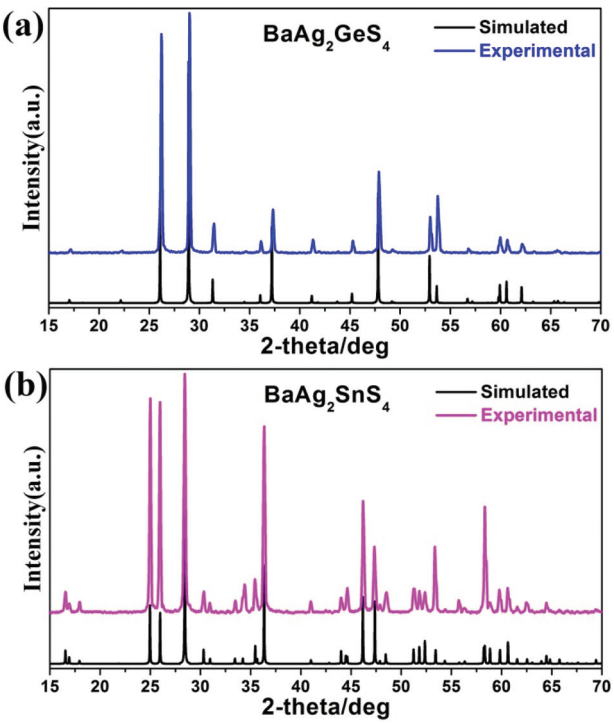

Fig. 1 Experimental and simulated PXRD patterns of (a) $BaAg_2GeS_4$ and (b) $BaAg_2SnS_4$.

phase was observed within the detection limits of the equipment. The title compounds appeared stable in air over periods of time longer than five months.

Crystal structure determinations

High-optical-quality title crystals were selected for the single-crystal XRD collection. All diffraction data were collected at room temperature on the Saturn 724 diffractometer with Mo-K_α radiation (λ = 0.71073 Å). The absorption corrections were performed and the structures were solved by direct methods[48] and refined by full-matrix least-squares fitting on F^2 by SHELX-2014 program package.[49] All the non-hydrogen atoms were refined with anisotropic thermal parameters and the coordinates were standardized using STRUCTURE TIDY.[50] Table 1 summarizes crystal data and structure refinements information for the title compounds, the atomic coordinates and isotropic displacement parameters are listed in Table S1† and the selected bond distances are listed in Table S2 in the ESI.†

Second harmonic generation (SHG) measurements

Powder SHG responses were measured on polycrystalline powder samples using a 2050 nm Q-switch laser based on a modified Kurtz-NLO system. The title compounds and reference crystalline AGS (2 × 2 × 3 cm^3 single crystals supplied from Anhui Institute of Optics and Fine Mechanics, CAS) were ground and sieved into a series of distinct particle size ranges (30–46, 46–74, 74–106, 106–150, 150–210 μm) to accomplish the size-dependent SHG signals, which was carried out as described elsewhere.[16,22,51]

Laser induced damage threshold (LIDT) measurements

Through the single-pulse measurement method,[52] powder LIDTs of polycrystalline title compounds at the range of 150–210 μm were investigated. AGS single crystals of similar size were chosen as the reference. Each sample was packed into a plastic holder (diameter: 8 mm; thickness: 1 mm). After being irradiated by the high-power 1064 nm laser radiation with a pulse width, τ_p, of 8 ns, the apparent change in the sample was monitored using an optical microscope. The power of laser beam was measured using a Nova II sensor equipped with a PE50-DIF-C energy sensor, and the size of the damage spot was measured using a Vernier caliper.

Computational sections

Theoretical studies were performed by the density functional theory (DFT)[53a] with the generalized gradient approximation (GGA)[53b] as implemented in the *Vienna ab initio simulation package* (VASP).[53c] The plane-wave basis with projector augmented wave (PAW)[53d,e] potentials was used to represent the core electrons. The plane-wave cut-off energy of 600 eV was chosen for all calculations and denser κ-point grids of 0.02 $Å^{-1}$ were carried out in the optical property calculations. For calculating the optical properties, scissors operators were applied for title compounds and AGS. The second-order nonlinear susceptibility $\chi^{abc(-2\omega,\ \omega,\ \omega)}$ was calculated through the so-called length-gauge formalism.[54] The specific parameter settings were described in our previously reported papers.[16,22,51]

Results and discussion

Structural description and comparison

Compounds **1** and **2** show the identical stoichiometry 1–2–1–4, but they belong to different crystal systems. Compound **1** crystallizes in the NCS tetragonal space group $I\bar{4}2m$ (no. 121) with $a = b$ = 6.820(9) Å, c = 8.021(2) Å, V = 373.1(2) $Å^3$, and Z = 2. Such crystal data are well-consistent with the previously reported phase.[45] In the structure, there are four crystallographically unique atoms, including one Ba atom (Wyckoff 2*b* special position), one Ag atom (Wyckoff 4*d* special position), one Ge atom (Wyckoff 2*a* special position) and one S atom (Wyckoff 8*i* special position) in the asymmetric unit. Compound **2** crystallizes in the NCS tetragonal space group *I*222 (no. 23) with a = 6.885(6) Å, b = 7.112(4) Å, c = 8.316(6) Å, V = 399.0(5) $Å^3$, and Z = 2. In the symmetric unit, each atom occupies one crystallographically unique position (Ba: Wyckoff 2*a*; Ag: Wyckoff 4*j*; Sn: Wyckoff 2*c*; S: Wyckoff 8*k*, respectively). It should be noted that such structural transformation comes from the simple element replacement (Ge to Sn), and the detailed symmetric operation change illustrated in Fig. 2 clearly shows the loss of the glide plane and the inversion axis from compound **1** to compound **2**. The symmetry breaking is accompanied by the decrease in symmetry elements from 8 to 4. Moreover, the space group *I*222 in compound **2** is a subgroup of $I\bar{4}2m$ in compound **1**, which has maximum non-isomorphic subgroups, including $I\bar{4}$, *Fmm*2, *I*222, $P\bar{4}21c$, $P\bar{4}21m$, $P\bar{4}2c$, and $P\bar{4}2m$. A similar structural change based on element substitution is also observed in the Ba–I_2–M^{IV}–Q_4 (I = Cu, Na; M^{IV} = Ge, Sn; Q = S, Se) system[44] and some other Ba-containing chalcogenides, *e.g.*, Ba_2BiGaS_5 *vs.* Ba_2BiInS_5 (*Pnma vs.*

Table 1 Crystallographic data and refinement details of $BaAg_2GeS_4$ and $BaAg_2SnS_4$

Formula	$BaAg_2GeS_4$	$BaAg_2SnS_4$
fw	553.91	600.01
Crystal system	Tetragonal	Orthorhombic
Crystal color	Red	Black
Space group	$I\bar{4}2m$ (no. 121)	*I*222 (no. 23)
a (Å)	6.820(9)	6.885(6)
b (Å)	6.820(9)	7.122(4)
c (Å)	8.021(2)	8.136(6)
α (°)	90	90
β (°)	90	90
γ (°)	90	90
V ($Å^3$)	373.1(2)	399.0(5)
Z	2	2
D_c (g cm^{-3})	4.93	4.99
μ (mm^{-1})	15.4	13.7
GOOF on F^2	1.004	1.005
R_1, wR_2 ($I > 2\sigma(I)$)[a]	0.0432, 0.1063	0.0452, 0.1160
R_1, wR_2 (all data)	0.0442, 0.1069	0.0494, 0.1166
Largest diff. peak and hole(e $Å^{-3}$)	2.241, −1.223	1.918, −2.494

[a] $R_1 = \sum||F_o| - |F_c||/\sum|F_o|$, $wR_2 = [\sum w(F_o^2 - F_c^2)^2/\sum w(F_o^2)^2]^{1/2}$.

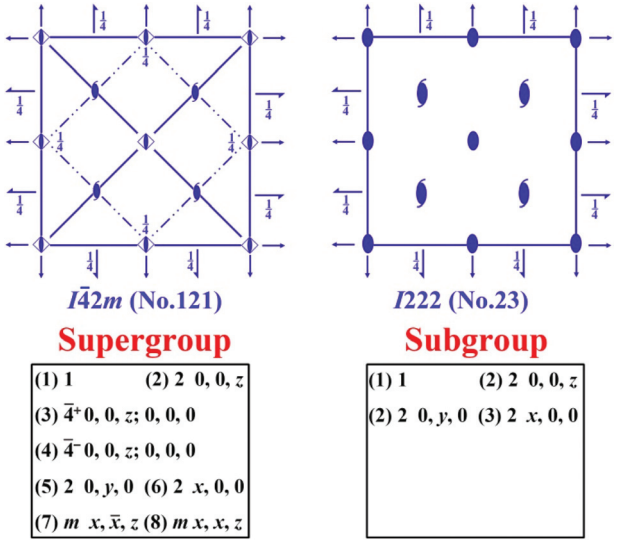

Fig. 2 Spatial symmetry operation change from supergroup $I\bar{4}2m$ (no. 121) to subgroup $I222$ (no. 23).

$Cmc2_1$),[55] $Ba_4Ga_2S_8$ *vs.* $Ba_4In_2S_8$ ($P\bar{1}$ *vs.* $P2_1$),[56] $Ba_2Ga_2S_5$ [57] *vs.* $Ba_2In_2S_5$ ($C2/c$ *vs.* $Pbca$)[58] and Ba_3GaS_4Cl[59] *vs.* Ba_3InS_4Cl ($Pnma$ *vs.* $I4/mcm$).[60]

As depicted in Fig. 3, the structural evolution of the title compounds $BaAg_2MS_4$ (M = Ge, Sn) is derived from the ternary chalcopyrite-like $AgGaS_2$ [space group: $I\bar{4}2d$ (no. 122), as shown in Fig. 3a] parent structure[61] by replacing the 2Ga cations with the M cations and with Ba^{2+} cations maintaining the charge balance. It can be observed from Fig. 3b that the basic structural unit of compound **1** is the two-dimensional (2D) Ag–S layer, which is composed of highly distorted AgS_4 tetrahedra connected with each other *via* corner-sharing. Such paralleled layers are further linked with the isolated GeS_4 tetrahedra by sharing corners to form a three-dimensional (3D) open tunnel structure along the *c* direction with Ba^{2+} cations located in the cavities. Compound **2** has a similar 3D tunnel structure to that of **1** except for their *b* and *c* axes interchanged (Fig. 3c). Of course, the different features in their structures are visible, for instance, the 2D straight Ag–S layer (*e.g.*, Ag–Ag–Ag angle is 90°) exists in compound **1**, while the wave-like Ag–S layer (*e.g.*, Ag–Ag–Ag angle is 81.3° or 98.7°) was observed in compound **2** (Fig. 4). The distorted AgS_4 tetrahedra have Ag–S distances of 2.594(3) Å for compound **1**, and 2.491(5)–2.786(5) Å for compound **2**, which are consistent with those of $BaAg_8S_5$ (2.438–2.905 Å),[62] $BaAgSbS_3$ (2.433–2.727 Å)[63] and $BaAgErS_3$ (2.542–2.748 Å).[64] Then, irregular MSe_4 (M = Ge, Sn) tetrahedra have typical $d_{(Ge-S)}$ = 2.210(4) Å in compound **1** and typical $d_{(Sn-S)}$ = 2.388(5) Å in compound **2**. Furthermore, the Ba atoms fill the 3D channels (Fig. 3b and c) and are present in the centre of the distorted S_8 polyhedra (Fig. 3c). The Ba–S interatomic distances vary from 3.251(5) to 3.307(6) Å in compound **1**, and from 3.292(6) to 3.337(6) Å in compound **2**, which is close to those of other related Ba-based sulfides, including $Ba_3KSb_4S_9Cl$ (3.169–3.449 Å),[65] $BaRh_2Ge_4S_6$ (3.289–3.361 Å)[66] and $Ba_3Ho_2P_4S_{16}$ (3.230–3.391 Å).[67] Taking compound **1** as an example, it is worth mentioning that the BaS_8 polyhedra in the different tunnels interlink together by sharing corners and edges to make up the 3D channel structure (Fig. 5a), but the BaS_8 polyhedra occupy discrete positions in the same tunnel (Fig. 5b).

Optical properties and thermal stabilities

The solid-state diffuse-reflectance UV–Vis–NIR spectra of title compounds were measured at room temperature, and the spectral results indicate that the experimental band gaps (E_g) are 2.02 eV for compound **1** and 1.77 eV for compound **2**, respectively (seen from Fig. 6a and b), which are consistent with their polycrystalline colours. Such values are smaller than that of benchmark AGS (E_g = 2.56 eV),[22] but still comparable to those of other commercial MFIR NLO materials, for instance, chalcopyrite-type semiconductors $AgGaSe_2$ (E_g = 1.75 eV)[6] and $ZnGeP_2$ (E_g = 1.65 eV).[7] As shown in Fig. 6c and d, results of TG and DTA measurements indicate that the compounds are thermally stable up to 1174 K for compound **1** and 1106 K for compound **2** under nitrogen atmosphere. In addition, the endothermic peak indicates that the title compounds decom-

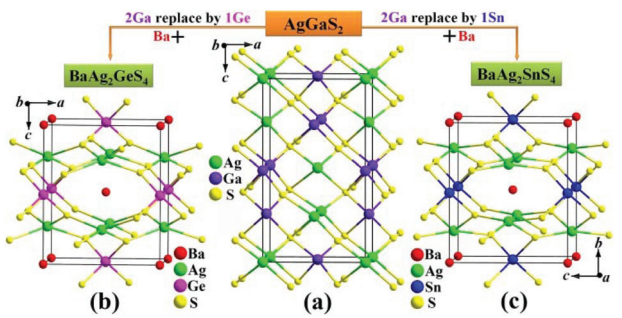

Fig. 3 Structural evolution from (a) classic chalcopyrite-type $AgGaS_2$ (SG: $I\bar{4}2d$) to the compressed chalcopyrite-like structure of (b) $BaAg_2GeS_4$ (SG: $I\bar{4}2m$) and (c) $BaAg_2SnS_4$ (SG: $I222$).

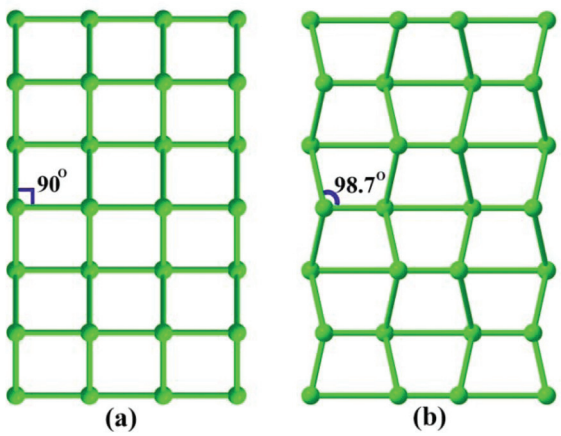

Fig. 4 The 2D straight Ag–S layer in compound **1** (a) and 2D wave-like Ag–S layer in compound **2** (b). The S atoms are omitted for a better view.

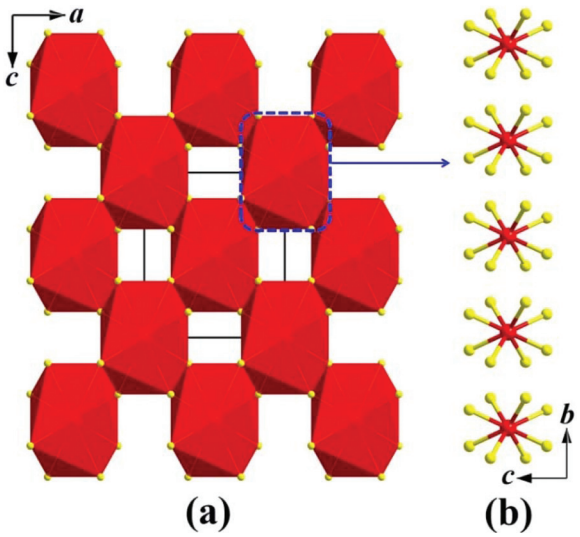

Fig. 5 (a) BaS_8 polyhedra *via* corner- and edge-sharing to make up the 3D framework structure in the *ac* plane with the unit cell marked. (b) Isolated BaS_8 polyhedra locate in the same tunnel (blue dashed-box) alone the *a*-axis.

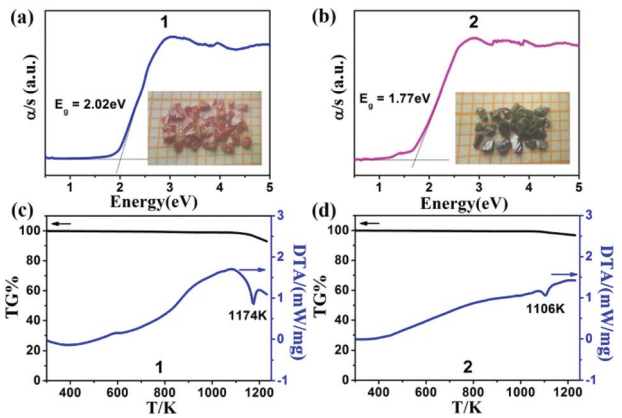

Fig. 6 Experimental results of compounds **1** and **2**: (a) and (b) are the solid-state UV–Vis–NIR optical absorption spectra, inserted are the photographs of title crystals; (c) and (d) are TG-DTA diagrams.

posed after this temperature, which is in accordance with the PXRD analysis (detailed information is given in ESI, Fig. S2†).

NLO properties and powder LIDTs

As the title compounds belong to a NCS space group ($I\bar{4}2m$ and $I222$), their powder SHG properties were systemically investigated in different particle sizes using the Kurtz and Perry method with 2050 nm Q-switch pulse laser and $AgGaS_2$ (AGS) as a benchmark material. As shown in Fig. 7a, the SHG responses of the two compounds increase with the increase in particle size, which indicates a type-I PM behavior. Compound **1** has a strong SHG intensity, which is about 1.7 times that of benchmark AGS at a particle size of 150–210 μm, while compound **2** shows the weak SHG response about 0.4 times of AGS in the same particle size.

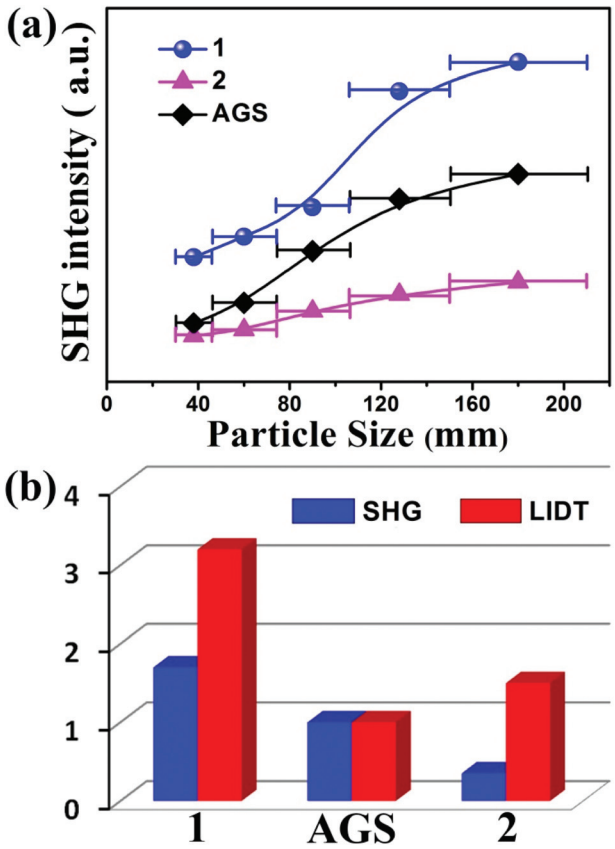

Fig. 7 (a) Particle size *vs.* SHG intensity curves for title compounds and AGS (reference) at 2050 nm radiation. The solid curves are drawn to guide the eyes and not fit to the data. (b) The relative SHG and LIDT intensities of title compounds and AGS in the particle size of 150–210 μm.

In recent years, estimating the LIDTs of novel MFIR NLO materials on powder sample has become a feasible and semi-quantitative method.[62] In this study, the powdered LIDTs of title compounds were systemically evaluated with AGS sample as the reference under a 1064 nm pulse laser, and the results are shown in Fig. 7b and listed in Table 1. Both of them show high LIDTs, and the measured values (4.61 and 2.16 MW cm^{-2}) are about 3.2 and 1.5 times that of powdered AGS (1.44 MW cm^{-2}), respectively. These data are comparable to those of exceptional MFIR NLO materials, such as powdered $BaNa_2SnS_4$ (1.0× AGS),[44a] powdered $BaLi_2MSe_4$ (M = Ge, Sn; 1.0× AGS),[44c] and powdered $AgGa_2PS_6$ (5.1× AGS),[34] and single-crystal $LiInS_2$ (2.5× AGS)[68] and single-crystal $BaGa_4S_7$ (3.0× AGS).[69]

Based on the above overall experimental results, title compounds can achieve the balance of two important NLO parameters (large SHG intensities and high LIDTs), which indicates that they are promising candidates for MFIR NLO application.

Theoretical studies

The theoretical electronic structures as well as linear and NLO properties were investigated using VASP software to better understand and analyse the structure–property relationship of

the title compounds. As shown in Fig. S3 in ESI,† the top of the valence band (VB) and bottom of the conduction band (CB) are located at different points for compounds **1** and **2**, which indicate that they are indirect band gap semiconductors. Calculated results show that the theoretical band gaps are 0.62 and 0.48 eV for compounds **1** and **2**, respectively. Such values are smaller than the measured values (2.02 and 1.77 eV) due to the discontinuity of the exchange correlation potential that underestimates the band gap in semiconductors and insulators.[70] In addition, the calculated partial densities of states (PDOSs) of title compounds with main contributions near the Fermi level (E_F) are shown in Fig. 8a.

Based on the PDOSs of compound **1**, in the VB region below the E_F, the Ag-4d and S-3p states dominating the VB-1 region are mixing with minor Ge-4s and Ge-4p states. Above the Fermi level, the CB-1 region is derived primarily from the S-3p and Ge-4s states mixing with small amounts of Ag-4d and Ge-4p states. The Ba atoms almost make no contribution around E_F and act as electron donors to stabilize the structure. As for the compound **2**, the PDOSs were also achieved and are similar to that of compound **1** as shown in Fig. 8b. Therefore, the band gap absorptions are primarily ascribed to the charge transitions from the S-3p states to Ag-4d, Ge-4s/Sn-5s, and Ge-4p/Sn-5p states.

Furthermore, the SHG coefficients (d_{ij}) for title compounds were also calculated, as the space group of compound **1** is $I\bar{4}2m$, which belongs to the class $\bar{4}2m$ and has two non-vanishing coefficients in the SHG tensors (d_{14} and d_{36}), of which only one is independent (d_{14}) under the restriction of Kleinman's symmetry.[71] In addition, compound **2** belongs to 222 point group that allows for three nonzero coefficients in the SHG tensor and only one is independent: $d_{14} = d_{25} = d_{36}$. Moreover, the cut-off energy, which depends on the largest second-order SHG tensor d_{14}, was investigated to understand the origin of the SHG component of title compounds. Fig. 8b shows that in the regions of VB-1 (dominated by S-3p and Ag-4d orbitals) and CB-2 (dominated by S-3p, Ag-4d and Ge(Sn)-ns/np orbitals), the d_{14} values are most sharply increased, which contribute primarily to the second-order NLO susceptibility. In other words, the NLO activities of title compounds originate from the condensation of AgS_4 and MS_4 (M = Ge, Sn) tetrahedral units that built the 3D CCL structures.

It should be noted that the calculated d_{14} coefficient for compound **1** (d_{14} = 15.7 pm V^{-1}) is close to AGS (d_{36} = 18.2 pm V^{-1}) at a wavelength of 2050 nm (*ca.* 0.61 eV), which is in accordance with the experimental observations (Fig. 9a). However, the SHG experimental observation (0.4× AGS) is smaller than the calculated value (d_{14} (2050 nm) = 14.5 pm V^{-1}) of compound **2**. Such low SHG intensity could be due to the narrow optical E_g (1.77 eV) and strong absorption of both fundamental light (2050 nm) and frequency-doubled light (1025 nm). Thus, in order to obtain the precise SHG signals of compound **2**, it is necessary to use a fundamental light source with a much longer wavelength (*e.g.*, CO_2 laser).

As shown in Fig. 9b, the calculated birefringence (Δn) values of compounds **1** and **2** are 0.198 and 0.052 at a wavelength of 2050 nm (*ca.* 0.61 eV), respectively; these values are clearly larger than that of AGS (Δn (2050 nm) = 0.039). The relatively large Δn values in the MFIR region indicate PM behaviors, which is consistent with the experimental observations (Fig. 7). Furthermore, the frequency-dependent dielectric function (ε), refractive index (n), absorption coefficient (α) and reflectivity (R) (Fig. S4–S5 in ESI†) were also investigated and several important parameters taken for comparison (including unit cell, space group, phase-matchability, Δn and the relative powder SHG and LIDT intensities) in the quaternary Ba–M^{I}_2–M^{IV}–Q_4 family and benchmark AGS are summarized in Table 2, indicating that the title compounds satisfy the key requirements as promising MFIR NLO materials.

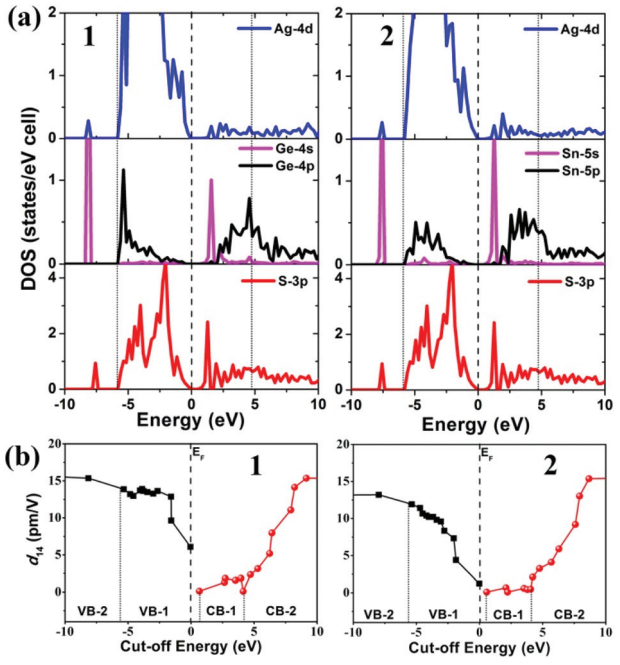

Fig. 8 (a) PDOSs of compounds **1** and **2** (the orbitals with minor contributions are omitted for clarity). (b) Static SHG coefficients of compounds **1** and **2** as a function of the cut-off energy. Dashed line, E_F; dotted line, different regions in valence bands (VB) and conduction bands (CB).

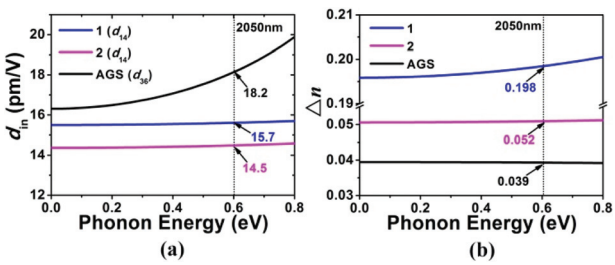

Fig. 9 (a) Calculated frequency-dependent SHG coefficients (d_{in}) and (b) calculated birefringence (Δn) for compounds **1** and **2** and AGS (as a reference).

Table 2 Structure-NLO property comparison in the quaternary $Ba–M^{I}_2–M^{IV}–Q_4$ family and benchmark $AgGaS_2$

Compounds	Unit cell	Space group	E_g (eV)	PM/NPM[a]	Calculated Δn	Powder SHG	Powder LIDT	Ref.
$AgGaS_2$	Tetragonal	$I\bar{4}2d$	2.56	PM	0.039	AGS	AGS	8 and 22
$BaLi_2GeS_4$	Tetragonal	$I\bar{4}2m$	3.66	PM	0.031	0.5× AGS	11× AGS	44*c*
$BaLi_2SnS_4$	Tetragonal	$I\bar{4}2m$	3.07	PM	0.033	0.7× AGS	6.5× AGS	
$BaLi_2GeSe_4$	Tetragonal	$I\bar{4}2m$	2.40	PM	0.038	1.1× AGS	1× AGS	
$BaLi_2SnSe_4$	Tetragonal	$I\bar{4}2m$	2.18	PM	0.066	1.3× AGS	1× AGS	
$BaNa_2GeS_4$	Trigonal	*R*3*c*	3.70	PM	0.037	0.3× AGS	8× AGS	44*a*
$BaNa_2SnS_4$	Tetragonal	$I\bar{4}2d$	3.27	PM	0.07	0.5× AGS	5× AGS	
$BaNa_2GeSe_4$	Trigonal	*R*3*c*	2.46	NPM	0.026	0.9× AGS	1× AGS	
$BaNa_2SnSe_4$	Trigonal	*R*3*c*	2.25	NPM	0.011	1.3× AGS	1× AGS	
$BaCu_2GeS_4$	Trigonal	$P3_121$	2.47	NPM	N/A	0.3× AGS	N/A	44*b*
$BaCu_2SnS_4$	Trigonal	$P3_221$	1.96	NPM	N/A	1.6× AGS	N/A	
$BaCu_2SiSe_4$	Trigonal	$P3_221$	2.62	NPM	N/A	0.3× AGS	N/A	
$BaCu_2GeSe_4$	Trigonal	$P3_121$	1.88	NPM	N/A	0.3× AGS	N/A	
$BaCu_2SnSe_4$	Orthorhombic	*Ama*2	1.72	NPM	N/A	0.3× AGS	N/A	
$BaAg_2GeS_4$	**Tetragonal**	$I\bar{4}2m$	**2.02**	**PM**	**0.198**	**1.7× AGS**	**3.2× AGS**	**This work**
$BaAg_2SnS_4$	**Orthorhombic**	***I*222**	**1.77**	**PM**	**0.052**	**0.4× AGS**	**1.5× AGS**	

[a] PM = phase-matchability, NPM = non-phase-matchability, and these are Type-I otherwise noted.

Conclusions

In summary, two new NCS compounds, $BaAg_2GeS_4$ (**1**) and $BaAg_2SnS_4$ (**2**), have been synthesized using the $BaCl_2$ flux method with high yields. Both these compounds exhibit compressed chalcopyrite-like structures compared with that of typical chalcopyrite-type $AgGaS_2$. For the first time, their NLO activities were discovered and systematically studied. It should be noted that the title compounds exhibit the type-I phase-matching abilities and excellent NLO performances, including strong SHG (1.7× and 0.4× $AgGaS_2$), high LIDTs (3.2× and 1.5× $AgGaS_2$) and large Δn (0.198 and 0.052), which indicates that they are promising candidates for NLO materials used in MFIR region. In addition, the Vienna *ab initio* theoretical studies show that the electronic transitions from S-3p states to Ag-4p and Ga-4p or Sn-4p states make the main contributions to the strong NLO activities for compounds **1** and **2**, respectively. Further efforts pursuing the growth of large-sized single crystals with good quality are in need.

Conflicts of interest

There are no conflicts to declare.

Acknowledgements

This work was supported by the National Natural Science Foundation of China (21771179, 21301175, 21233009, 21571020 and 91422303), the Major State Basic Research Development Program of China (973 Program, no. 2014CB845603), the Strategic Priority Research Program of the Chinese Academy of Sciences (no. XDB20010200), and the Natural Science Foundation of Fujian Province (2015J01071). We thank Professor Yong-Fan Zhang at Fuzhou University for helping with the DFT calculations.

Notes and references

1 (*a*) D. N. Nikogosyan, *Nonlinear Optical Crystals: A Complete Survey*, Springer-Science, New York, 2005; (*b*) X.-T. Wu and L. Chen, *Structure–Property Relationships in Nonlinear Optical Crystals II The IR Region*, In Structure and Bonding; D. M. Mingos, Series Ed., Springer, New York, 2012, vol. 145; (*c*) I. Chung and M. G. Kanatzidis, *Chem. Mater.*, 2014, **26**, 849–869; (*d*) C. L. Hu and J. G. Mao, *Coord. Chem. Rev.*, 2015, **288**, 1–17; (*e*) Y. Wang and S. L. Pan, *Coord. Chem. Rev.*, 2016, **323**, 15–35; (*f*) F. Liang, L. Kang, Z. S. Lin, Y. C. Wu and C. T. Chen, *Coord. Chem. Rev.*, 2017, **333**, 57–70; (*g*) S. P. Guo, Y. Chi and G. C. Guo, *Coord. Chem. Rev.*, 2017, **335**, 44–57; (*h*) W. W. Xiong and Q. C. Zhang, *Angew. Chem., Int. Ed.*, 2015, **54**, 11616–11623; (*i*) X. X. Li, Y. X. Wang, R. H. Wang, C. Y. Cui, C. B. Tian and G. Y. Yang, *Angew. Chem., Int. Ed.*, 2016, **55**, 6462–6466.
2 J. F. Ward and P. A. Franken, *Phys. Rev. [Sect.] A*, 1964, **133**, 183–190.
3 C. T. Chen, B. C. Wu, A. D. Jiang and G. M. You, *Sci. Sin., Ser. B*, 1985, **28**, 235–243.
4 C. T. Chen, Y. C. Wu, A. D. Jiang, B. Wu, G. M. You, R. K. Li and S. J. Lin, *J. Opt. Soc. Am. B*, 1989, **6**, 616–621.
5 R. C. Miller and W. A. Nordland, *Phys. Rev. B: Solid State*, 1970, **2**, 4896–4902.
6 G. D. Boyd, E. Buehler and F. G. Storz, *Appl. Phys. Lett.*, 1971, **18**, 301–304.
7 A. Harasaki and K. Kato, *Jpn. J. Appl. Phys.*, 1997, **36**, 700–703.
8 G. C. Catella, L. R. Shiozawa, J. R. Hietanen, R. C. Eckardt, R. K. Route, R. S. Feigelson, D. G. Cooper and C. L. Marquardt, *Appl. Opt.*, 1993, **32**, 3948–3951.
9 (*a*) A. Jayaraman, V. Narayanamurti, H. M. Kasper, M. A. Chin and R. G. Maines, *Phys. Rev. B: Solid State*, 1976, **14**, 3516–3519; (*b*) P. G. Schunemann, *AIP Conf. Proc.*, 2007, **916**, 541–559.
10 Y. Kim, I. Seo, S. W. Martin, J. Back, P. S. Halasyamani, N. Arumugam and H. Steinfink, *Chem. Mater.*, 2008, **20**, 6048–6052.

11 J. A. Brant, D. J. Clark, Y. S. Kim, J. I. Jang, J. H. Zhang and J. A. Aitken, *Chem. Mater.*, 2014, **26**, 3045–3048.
12 K. Wu, Z. H. Yang and S. L. Pan, *Chem. Commun.*, 2017, **53**, 3010–3013.
13 G. M. Li, K. Wu, Q. Liu, Z. H. Yang and S. L. Pan, *J. Am. Chem. Soc.*, 2016, **138**, 7422–7428.
14 S. F. Li, X. M. Jiang, B. W. Liu, D. Yan, C. S. Lin, H. Y. Zeng and G. C. Guo, *Chem. Mater.*, 2017, **29**, 1796–1804.
15 I. Chung, J. H. Song, J. I. Jang, A. J. Freeman, J. B. Ketterson and M. G. Kanatzidis, *J. Am. Chem. Soc.*, 2009, **131**, 2647–2656.
16 H. Lin, L. Chen, J. S. Yu, H. Chen and L. M. Wu, *Chem. Mater.*, 2017, **29**, 499–503.
17 (*a*) S. Banerjee, C. D. Malliakas, J. I. Jang, J. B. Ketterson and M. G. Kanatzidis, *J. Am. Chem. Soc.*, 2008, **130**, 12270–12272; (*b*) S. Banerjee, J. M. Szarko, B. D. Yuhas, C. D. Malliakas, L. X. Chen and M. G. Kanatzidis, *J. Am. Chem. Soc.*, 2010, **132**, 5348–5350.
18 T. K. Bera, J. I. Jang, J. B. Ketterson and M. G. Kanatzidis, *J. Am. Chem. Soc.*, 2009, **131**, 75–77.
19 C. D. Morris, I. Chung, S. Park, C. M. Harrison, D. J. Clark, J. I. Jang and M. G. Kanatzidis, *J. Am. Chem. Soc.*, 2012, **134**, 20733–20744.
20 (*a*) J.-H. Liao, G. M. Marking, K. F. Hsu, Y. Matsushita, M. D. Ewbank, R. Borwick, P. Cunningham, M. J. Rosker and M. G. Kanatzidis, *J. Am. Chem. Soc.*, 2003, **125**, 9484–9493; (*b*) K. Wu, Z. H. Yang and S. L. Pan, *Chem. Mater.*, 2016, **28**, 2795–2801.
21 B. W. Liu, H. Y. Zeng, X. M. Jiang, G. E. Wang, S. F. Li, L. Xu and G. C. Guo, *Chem. Sci.*, 2016, **7**, 6273–6277.
22 (*a*) H. Lin, L. J. Zhou and L. Chen, *Chem. Mater.*, 2012, **24**, 3406–3414; (*b*) H. Lin, L. Chen, L. J. Zhou and L. M. Wu, *J. Am. Chem. Soc.*, 2013, **135**, 12914–12921; (*c*) M. L. Zhou, Y. Yang, Y. W. Guo, Z. S. Lin, J. Y. Yao, Y. C. Wu and C. T. Chen, *Chem. Mater.*, 2017, **29**, 7993–8002; (*d*) H. Lin, H. Chen, Y. J. Zheng, J. S. Yu, X. T. Wu and L. M. Wu, *Chem. – Eur. J.*, 2017, **23**, 10407–10412.
23 Z. Z. Luo, C. S. Lin, H. H. Cui, W. L. Zhang, H. Zhang, H. Chen, Z. Z. He and W. D. Cheng, *Chem. Mater.*, 2015, **27**, 914–922.
24 R. H. Duan, P. F. Liu, H. Lin, Y. J. Zheng, J. S. Yu, X. T. Wu, S. X. Huang-Fu and L. Chen, *J. Mater. Chem. C*, 2017, **5**, 7067–7074.
25 M. C. Chen, L. M. Wu, H. Lin, L. J. Zhou and L. Chen, *J. Am. Chem. Soc.*, 2012, **134**, 6058–6060.
26 S.-M. Kuo, Y.-M. Chang, I. Chung, J.-I. Jang, B.-H. Her, S.-H. Yang, J. B. Ketterson, M. G. Kanatzidis and K.-F. Hsu, *Chem. Mater.*, 2013, **25**, 2427–2433.
27 W. H. Lai, A. S. Haynes, L. Frazer, Y. M. Chang, T. K. Liu, J. F. Lin, I. C. Liang, H. S. Sheu, J. B. Ketterson, M. G. Kanatzidis and K. F. Hsu, *Chem. Mater.*, 2015, **27**, 1316–1326.
28 X. S. Li, C. Li, P. F. Gong, Z. S. Lin, J. Y. Yao and Y. C. Wu, *J. Mater. Chem. C*, 2015, **3**, 10998–11004.
29 W. L. Yin, A. K. Iyer, C. Li, J. Y. Yao and A. Mar, *J. Mater. Chem. C*, 2017, **5**, 1057–1063.
30 Y. Y. Li, P. F. Liu and L. M. Wu, *Chem. Mater.*, 2017, **29**, 5259–5266.
31 M. C. Chen, L. H. Li, Y. B. Chen and L. Chen, *J. Am. Chem. Soc.*, 2011, **133**, 4617–4624.
32 H. J. Zhao, Y. F. Zhang and L. Chen, *J. Am. Chem. Soc.*, 2012, **134**, 1993–1995.
33 Y. F. Shi, Y. K. Chen, M. C. Chen, L. M. Wu, H. Lin, L. J. Zhou and L. Chen, *Chem. Mater.*, 2015, **27**, 1876–1884.
34 J. H. Feng, C. L. Hu, X. Xu, B. X. Li, M. J. Zhang and J. G. Mao, *Chem. – Eur. J.*, 2017, **23**, 10978–10982.
35 Q. C. Zhang, I. Chung, J. I. Jang, J. B. Ketterson and M. G. Kanatzidis, *Chem. Mater.*, 2009, **21**, 12–14.
36 W. W. Xiong, E. U. Athresh, Y. T. Ng, J. F. Ding, T. Wu and Q. C. Zhang, *J. Am. Chem. Soc.*, 2013, **135**, 1256–1259.
37 Y. Liu, F. X. Wei, S. N. Yeo, F. M. Lee, C. Kloc, Q. Y. Yan, H. H. Hng, J. Ma and Q. C. Zhang, *Inorg. Chem.*, 2012, **51**, 4414–4416.
38 C. Liu, Y. Y. Shen, P. P. Hou, M. J. Zhi, C. M. Zhou, W. X. Chai, J. W. Cheng and Y. Liu, *Inorg. Chem.*, 2015, **54**, 8931–8936.
39 W. W. Xiong, J. W. Miao, K. Q. Ye, Y. Wang, B. Liu and Q. C. Zhang, *Angew. Chem., Int. Ed.*, 2015, **54**, 546–550.
40 D. M. Yan, C. Liu, W. X. Chai, X. R. Zhang, L. D. Zhang, M. J. Zhi, C. M. Zhou, Q. C. Zhang and Y. Liu, *Chem. – Asian J.*, 2016, **11**, 1842–1848.
41 L. Xu, H. Zhu, G. K. Long, J. Zhao, D. S. Li, R. Ganguly, Y. X. Li, Q. H. Xu and Q. C. Zhang, *J. Mater. Chem. C*, 2015, **3**, 9191–9196.
42 X. X. Li, X. Ma, W. X. Zheng, Y. J. Qi, S. T. Zheng and G. Y. Yang, *Inorg. Chem.*, 2016, **55**, 8257–8259.
43 C. Liu, P. P. Hou, W. X. Chai, J. W. Tian, X. R. Zhang, Y. Y. Shen, M. J. Zhi, C. M. Zhou and Y. Liu, *J. Alloys Compd.*, 2016, **679**, 420–425.
44 (*a*) K. Wu, Z. H. Yang and S. L. Pan, *Angew. Chem., Int. Ed.*, 2016, **55**, 6713–6715; (*b*) L. Y. Nian, J. B. Huang, K. Wu, Z. Su, Z. H. Yang and S. L. Pan, *RSC Adv.*, 2017, **7**, 29378–29385; (*c*) K. Wu, B. B. Zhang, Z. H. Yang and S. L. Pan, *J. Am. Chem. Soc.*, 2017, **139**, 14885–14888.
45 C. L. Teske and O. Vetter, *Z. Anorg. Allg. Chem.*, 1976, **427**, 200–204.
46 C. L. Teske, *Z. Naturforsch., B: Anorg. Chem., Org. Chem.*, 1979, **34**, 544–547.
47 P. Kubelka, *Z. Tech. Phys.*, 1931, **12**, 593–601.
48 *Crystal Clear, version 1.3.5*, Rigaku Corp., The Woodlands, TX, 1999.
49 G. M. Sheldrick, *Acta Crystallogr., Sect. A: Found. Crystallogr.*, 2008, 112–122.
50 L. M. Gelato and E. Parthe, *J. Appl. Crystallogr.*, 1987, **20**, 139–143.
51 (*a*) H. Lin, Y. Liu, L. J. Zhou, H. J. Zhao and L. Chen, *Inorg. Chem.*, 2016, **55**, 4470–4475; (*b*) H. Lin, H. Chen, Y. J. Zheng, J. S. Yu and L. M. Wu, *Dalton Trans.*, 2016, **45**, 17606–17609; (*c*) H. Lin, Y. J. Zheng, H. Chen, X. N. Hu, J. S. Yu and L. M. Wu, *Chem. – Asian J.*, 2017, **12**, 453–458.
52 M. J. Zhang, X. M. Jiang, L. J. Zhou and G. C. Guo, *J. Mater. Chem. C*, 2013, **1**, 4754–4760.

53 (*a*) G. Kresse and J. Furthmuller, *Phys. Rev. B: Condens. Matter Mater. Phys.*, 1996, **54**, 11169–11186; (*b*) J. P. Perdew and Y. Wang, *Phys. Rev. B: Condens. Matter Mater. Phys.*, 1992, **45**, 13244–13249; (*c*) G. Kresse and D. Joubert, *Phys. Rev. B: Condens. Matter Mater. Phys.*, 1999, **59**, 1758–1775; (*d*) P. E. Blöchl, *Phys. Rev. B: Condens. Matter Mater. Phys.*, 1994, **50**, 17953–17979; (*e*) P. E. Blöchl, O. Jepsen and O. K. Andersen, *Phys. Rev. B: Condens. Matter Mater. Phys.*, 1994, **49**, 16223–16234.

54 (*a*) C. Aversa and J. E. Sipe, *Phys. Rev. B: Condens. Matter Mater. Phys.*, 1995, **52**, 14636–14645; (*b*) S. N. Rashkeev, W. R. L. Lambrecht and B. Segall, *Phys. Rev. B: Condens. Matter Mater. Phys.*, 1998, **57**, 3905–3919.

55 L. Geng, W.-D. Cheng, C.-S. Lin, W.-L. Zhang, H. Zhang and Z.-Z. He, *Inorg. Chem.*, 2011, **50**, 5679–5686.

56 J. W. Liu, P. Wang and L. Chen, *Inorg. Chem.*, 2011, **50**, 5706–5713.

57 B. Eisenmann, M. Jakowski and H. Schäfer, *Z. Naturforsch.*, 1983, **38b**, 1581–1584.

58 B. Eisenmann and A. Hofmann, *Z. Anorg. Allg. Chem.*, 1990, **580**, 151–159.

59 K. Feng, W. L. Yin, Z. H. Lin, J. Y. Yao and Y. C. Wu, *Inorg. Chem.*, 2013, **52**, 11503–11508.

60 M. Y. Pan, S. Q. Xia, X. C. Liu and X. T. Tao, *J. Solid State Chem.*, 2014, **219**, 74–79.

61 S. Laksari, A. Chahed, N. Abbouni, O. Benhelal and B. Abbar, *Comput. Mater. Sci.*, 2006, **38**, 223–230.

62 C. E. Check, C. Zheng, J. H. Zhang and B. Dabrowski, *J. Solid State Chem.*, 1999, **144**, 409–415.

63 C. Liu, Y. Y. Shen, P. P. Hou, M. J. Zhi, C. M. Zhou, W. X. Chai, J.-W. Cheng and Y. Liu, *Inorg. Chem.*, 2015, **54**, 8931–8936.

64 P. Wu and J. A. Ibers, *J. Solid State Chem.*, 1994, **110**, 156–161.

65 H. J. Zhao and P. F. Liu, *J. Solid State Chem.*, 2015, **232**, 37–41.

66 H. C. Lei, J. I. Yamaura, J. G. Guo, Y. P. Qi, Y. Toda and H. Hosono, *Inorg. Chem.*, 2014, **53**, 5684–5691.

67 Y. Klawitter, W. Bensch and C. Wickleder, *Chem. Mater.*, 2006, **18**, 187–197.

68 G. M. H. Knippels, A. F. G. van der Meer, A. M. MacLeod, A. Yelisseyev, L. Isaenko, S. Lobanov, I. Thenot and J. J. Zondy, *Opt. Lett.*, 2001, **26**, 617–619.

69 X. S. Lin, G. Zhang and N. Ye, *Cryst. Growth Des.*, 2009, **9**, 1186–1189.

70 J. P. Perdew, K. Burke and M. Ernzerhof, *Phys. Rev. Lett.*, 1996, **77**, 3865–3868.

71 D. A. Kleinman, *Phys. Rev.*, 1962, **126**, 1977–1979.